[CANCER RESEARCH 60, 4953–4958, September 1, 2000]

In Vivo Imaging of Proteolytic Enzyme Activity Using a Novel Molecular Reporter[1]

Ching-Hsuan Tung, Umar Mahmood, Sebastian Bredow, and Ralph Weissleder[2]

Center for Molecular Imaging Research, Massachusetts General Hospital, Harvard Medical School, Charlestown, Massachusetts 02129

ABSTRACT

The single biggest challenge facing *in vivo* imaging techniques is to develop biocompatible molecular beacons that are capable of specifically and accurately measuring *in vivo* targets at the protein, RNA, or DNA level. Our efforts have focused on developing activatable imaging probes to measure specific enzyme activities *in vivo*. Using cathepsin D as a model target protease, we synthesized a long-circulating, synthetic graft copolymer bearing near-infrared (NIR) fluorochromes positioned on cleavable substrate sequences. In its native state, the reporter probe was essentially nonfluorescent at 700 nm due to energy resonance transfer among the bound fluorochromes (quenching) but became brightly fluorescent when the latter were released by cathepsin D. NIR fluorescence signal activation was linear over at least 4 orders of magnitude and specific when compared with scrambled nonsense substrates. Using matched rodent tumor models implanted into nude mice expressing or lacking the targeted protease, it could be shown that the former generated sufficient NIR signal to be directly detectable and that the signal was significantly different compared with negative control tumors. The developed probes should find widespread applications for real-time *in vivo* imaging of a variety of clinically relevant proteases, for example, to detect endogenous protease activity in disease, to monitor the efficacy of protease inhibitors, or to image transgene expression.

INTRODUCTION

There is a growing need in the medical imaging sciences to better detect and characterize abnormal tissue and disease processes and to directly image protein expression. Because most clinical imaging systems rely on physical parameters to generate image contrast (*e.g.*, acoustic impedance, magnetic properties, X-ray absorption, and optical absorption or reflectance), specific molecular information can often not be obtained or is of limited nature. Optical imaging in the NIR[3] spectrum offers the possibility of using fluorescence-tagged reporter probes, injectable i.v., to impart molecular specificity. Unlike other reporters, fluorescent probes can be physically quenched to minimize signal in the nonactivated state while becoming brightly fluorescent after specific molecular conformational changes (1) or reactions (2). Although a variety of such "caged" probes exist for *in vitro* diagnosis (3), it has not been until very recently that probes for *in vivo* use have been developed that are activated by a variety of nonspecific lysosomal proteases (4). However, real-time detection of single specific enzymes and pathways *in vivo* has been largely elusive to date.

We hypothesized that specific biocompatible reporter probes can be synthesized to image single target proteases *in vivo*. We attached NIRF fluorochromes through specific peptide substrates directly to a delivery vehicle (Fig. 1). Although it is conceivable to design alternative low molecular weight probes in which a fluorescence donor and a quencher are directly attached to a substrate peptide (2, 5), such compounds are typically subject to fast excretion *in vivo*. For this reason, and to improve tumoral delivery of the NIRF probes, we used a novel, long-circulating synthetic PGC that has recently been tested in clinical trials (6). The copolymer accumulates in tumors by slow extravasation through permeable neovasculature, reaching up to 2–6% injected dose/g tissue in mice within 24–48 h after injection in some tumor models (7). Uptake of the polymer into tumor cells occurs by pinocytosis and is comparable in magnitude to that of tumor-specific internalizing monoclonal antibodies. The intracellular release of NIRF probes results in a fluorescent signal that can be detected *in vivo* at subnanomolar quantities and at depths sufficient for experimental or clinical imaging, depending on the NIRF image acquisition technique (4).

To test the hypothesis that specific enzyme activity can be imaged *in vivo*, a rodent tumor model system was used. The 3Y1 tumor has a very low level of rodent CaD, whereas a stable clone expressing hCaD has recently been generated (8, 9); CaD may be relevant to metastagenesis (10). Both tumors were implanted into mice and probed with an i.v. injected reporter probe specific for CaD. In this report, we demonstrate for the first time that CaD enzyme activity can be directly imaged *in vivo*. This novel technique should find several applications to measure a variety of enzyme activities noninvasively in normal tissues during disease development and during protease inhibitor treatments.

MATERIALS AND METHODS

Synthesis and Assay. A PGC (11) was used as a delivery vehicle for the fluorochrome-peptide conjugate (Fig. 1). The structure, physicochemical characteristics, and biological behavior of the graft copolymer have been described previously, and a similar compound has been tested in clinical trials (6). The preparation of the entire NIRF probe has been described in more detail elsewhere (12). Briefly, PGC (M_r 450,000) was reacted with a large excess of iodoacetyl anhydride (Aldrich, Milwaukee, WI) to convert all available amino groups of the poly-L-lysine backbone into iodol groups. The CaD-specific peptide Gly-*Pro-Ile-Cys(Et)-Phe-Phe-Arg-Leu*-Gly-Lys(FITC)-Cys-NH_2 [the *italicized amino acids* correspond to CaD substrate (5)] was synthesized using an automatic synthesizer (PS3; Rainin, Woburn, MA). *N*-(9-Fluorenyl)methoxycarbonyl chemistry with 2-(1*H*-benzotriazole-1-yl)-1,1,3,3-tetramethyluronium hexafluorophosphate/*N*-hydroxybenzotriazole as the activating agent was used in peptide synthesis. The purified and characterized peptide was then attached to the iodoacetylated PGC through a thiol-specific reaction. The NIRF dye Cy5.5 (Amersham, Arlington Heights, IL) was subsequently conjugated to the N-terminus of the CaD substrate peptide. Peptide and fluorochrome attachment was quantitated by absorption measurements of FITC and Cy 5.5. Extinction coefficients were 73×10^3 $M^{-1}cm^{-1}$ at 494 nm for FITC and 250×10^3 $M^{-1}cm^{-1}$ at 675 nm for Cy5.5. On average, each graft copolymer contained 22 NIRF reporter groups, as determined by fluorescence measurements. The calculated molecular weight of the entire probe is 490,000.

To test the specificity of the developed probe, 0.2 μM of the CaD-sensitive probe and a nonsense scrambled control peptide-based probe [Gly-Pro-Phe-Cys(Et)-Ile-Arg-Phe-Leu-Gly-Lys(FITC)-Cys-NH_2; Ref. 12] were treated with 1 unit of hCaD (Sigma, St. Louis, MO) in 1 ml of 50 mM glycine/hydrochloride buffer (pH 3.5) with 0.001% Brij-35. The fluorescence activation of the two

Received 3/29/00; accepted 6/27/00.

The costs of publication of this article were defrayed in part by the payment of page charges. This article must therefore be hereby marked *advertisement* in accordance with 18 U.S.C. Section 1734 solely to indicate this fact.

[1] Supported in part by National Institute of Diabetes and Digestive and Kidney Diseases Grant R21-DK55713-01, the Massachusetts General Hospital-Center for Molecular Imaging Research Development Fund, and a grant from the Massachusetts General Hospital Center for Innovative Minimally Invasive Therapy.

[2] To whom requests for reprints should be addressed, at Center for Molecular Imaging Research, Massachusetts General Hospital, Building 149, Room 5403, Charlestown, MA 02129. Phone: (617) 726-8226; Fax: (617) 726-5708; E-mail: weissleder@helix.mgh.harvard.edu.

[3] The abbreviations used are: NIR, near-infrared; NIRF, NIR fluorescence; PGC, poly-L-lysine/methoxypolyethylene glycol graft copolymer; CaD, cathepsin D; hCaD, human CaD; RT-PCR, reverse transcription-PCR; CCD, charge-coupled device; CNR, contrast:noise ratio; MMP, matrix metalloproteinase; SI, signal intensity.

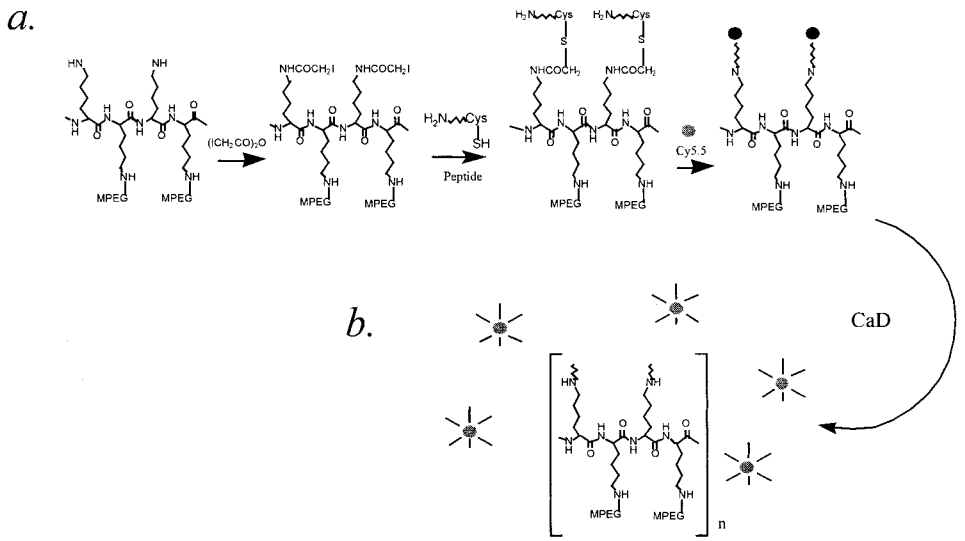

Fig. 1. Schematic diagram of the synthesis (*a*) and activation (*b*) of the developed reporter probe. The delivery vehicle consists of a partially methoxy-pegylated poly-L-lysine graft copolymer. CaD peptide substrates are conjugated to remaining lysines on the polymer backbone through an acetyl linker and are subsequently modified with Cy5.5 fluorochromes (*circles*). The NIRF of the native reporter compound is minimal (<1 AU). On interaction with CaD, Cy5.5 is released from the peptide substrate, causing a >60-fold increase in the NIRF signal.

probes was measured by fluorometry [excitation:emission = 675:694 nm; (U4500; Hitachi, Tokyo, Japan)].

Cell Culture. Two rodent rat embryo tumor cell lines (3Y1) were kindly provided by Drs. H. Rochefort and M. Garcia [Institut National de la Santé et de la Recherche Médicale, Montpellier, France (8, 9)]. One of the cell lines was stably transfected with full-length hCaD (CaD+), whereas the other cell line was mock-transfected with an empty expression vector, resulting in no hCaD expression (CaD−; Fig. 2). These rodent cell lines were initially chosen for transfection because they neither produce nor secrete rodent CaD. Both cell lines were grown in RPMI 1640 supplemented with 10% fetal bovine serum and 0.4 mg/ml G418 in a humidified 6% CO_2 atmosphere at 37°C (9).

The NIRF probe was tested in cell culture using CaD+ cells grown to confluence on glass coverslips. Prior to experiments, the culture medium on coverslips was replaced with 500 μl of fresh medium containing 1 μM NIRF probe. After 1 h at 37°C, cells were washed three times and then subjected to fluorescence microscopy using a confocal microscope (TCS 4D; Leica, Deerfield, IL). To test the linearity of NIRF activation as a function of enzyme activity, varying amounts of CaD+ cells (10^3 to 10^6 cells) were incubated with 1 μM reporter probe at 37°C for 30 min. The cells were then washed three times with fresh medium and harvested, and NIRF generation was detected in intact cells using a fluorometer (U4500; Hitachi).

To induce solid tumors, 1.5×10^6 cells were injected s.c. into the lateral lower abdomen of nude mice ($n = 5$). Tumor implantations were performed 1 week apart because the CaD+ tumor demonstrated a slightly faster growth rate. Within 2–3 weeks after the last implantation, each mouse had developed both CaD+ and CaD− tumors of 5–12 mm in size.

Assays for CaD Expression. Expression of hCaD (or lack thereof in the mock-transfected cell line) was verified by Western blotting and RT-PCR. For the latter, previously described primers (13) were used at 0.2 μM and at a cDNA equivalent of 7 ng of RNA. Combined annealing and extension were performed at 72°C for 150 s. Control PCR experiments for the housekeeping gene β-actin were performed on the same samples using commercially available primers (Clontech, Palo Alto, CA). Cycle numbers for the individual products were 34–36 for CaD and 20–22 for β-actin. PCR products were analyzed by electrophoresis on 2% agarose gels. Gels were photographed using a Kodak DC 40 system and analyzed with BioMax software (Kodak, Rochester, NY).

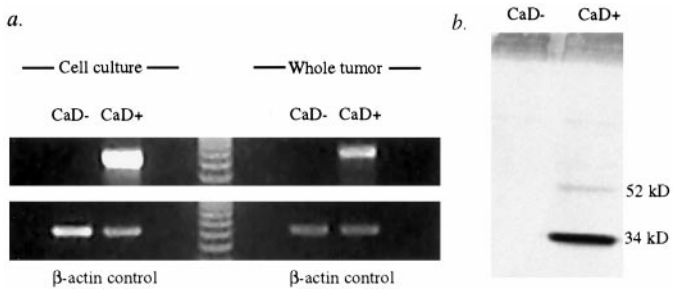

Fig. 2. Characterization of tumor models by RT-PCR (*a*) and Western blotting (*b*). RT-PCR shows positive mRNA signals in the stably transfected CaD+ cell line and no signal in the control cell line transfected with an empty expression vector; (*b*) Western blotting shows a strong M_r 34,000 band corresponding to activated CaD and a weaker M_r 52,000 band corresponding to pro-CaD.

For Western blotting, cells were lysed in 2 ml of buffer [20 mM Tris (pH 8.0), 150 mM NaCl, 5 mM EDTA, and 1% Triton X-100]. The lysate was kept on ice for 20 min and then centrifuged for 10 min at 4°C at 16,000 × *g*. Protein concentration was determined by the BCA assay (Pierce, Rockford, IL). Equal amounts of protein were loaded and electrophoretically separated by SDS-PAGE in nonreducing 10% gels. After transfer onto polyvinylidene difluoride membranes, immunoblots were incubated for 30 min with an anti-hCaD polyclonal antibody (Calbiochem, San Diego, CA) for 30 min. The primary antibody was revealed with an alkaline phosphatase-conjugated goat antirabbit IgG secondary antibody (Sigma) using nitroblue tetrazolium/5-bromo-4-chloro-3-indolyl phosphate substrate (Boehringer Mannheim, Indianapolis, IN).

***In Vivo* Imaging.** The imaging system used in this study consisted of a light-tight imaging chamber equipped with a 150 W halogen white light filtered with an excitation bandpass filter (610–650 nm; Omega Optical, Brattleboro, VT; Ref. 14) to excite Cy5.5. Fiberoptic cables and light diffusers resulted in a relatively spatially homogenous photon source over the imaging area. Fluorescence was detected by a 12-bit monochrome CCD camera (Kodak) equipped with a f/1.2 12.5–75 mm zoom lens and an emission long pass filter at 700 nm (Omega Optical). Images were digitally acquired and saved as 16-bit Tiff files.

Anesthetized mice ($n = 5$) were imaged 24 h after i.v. injection of 2.5 nmol of fluorochrome (corresponding to 2.5 mg/kg probe). To further analyze *in vivo* imaging findings, each tumor pair excised from a single animal was also imaged after excision. Image analysis was performed using commercially available software (Kodak Digital Science 1D software, Rochester, NY). Elliptical regions of interest were selected manually for tumor center and tumor periphery for CaD+ and for entire CaD− tumors, as well as for representative adjacent nontarget tissue (adjacent thigh). The mean and SD of SI of pixel values was recorded. CNRs were calculated for each animal. Significance of differences among groups was determined using a one-tailed Student's *t* test.

Histology. Harvested tumors were snap frozen in liquid nitrogen and cut into 8–20-μm sections. Immunohistochemistry was performed using a primary rabbit polyclonal antibody against hCaD (Dako, Carpinteria, CA). The primary antibody was revealed with a goat antirabbit antibody conjugated to alkaline phosphatase. After a heat step (65°C, 30 min), phosphatase activity was visualized using nitroblue tetrazolium/5-bromo-4-chloro-3-indolyl phosphate substrate, and sections were counterstained with nuclear fast red. CaD expression was also assessed on nonfixed 20-μm sections by NIRF microscopy using

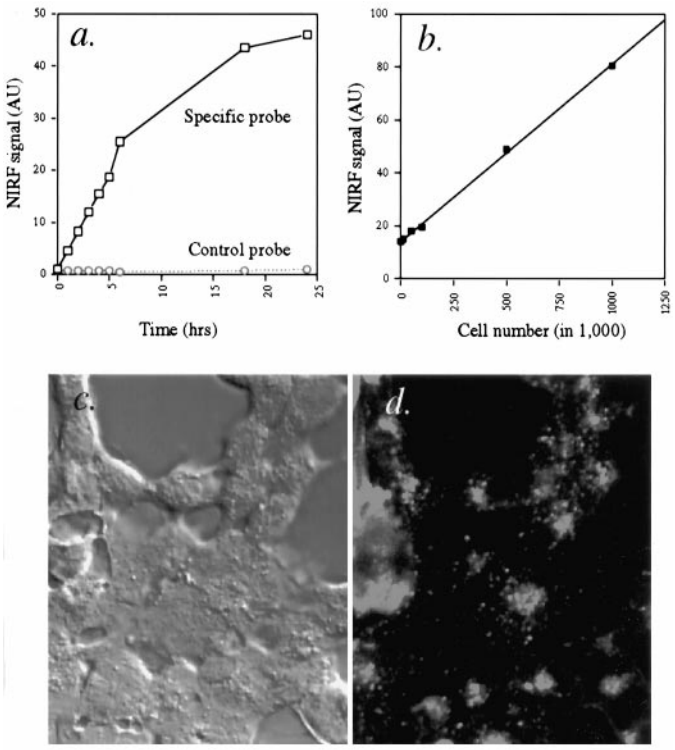

Fig. 3. *a*, NIRF signal generation as a function of time with the CaD-sensitive probe compared with a scrambled peptide probe. *b*, linearity of enzyme-mediated NIRF signal generated by incubating varying amounts of cells with 1.0 μM CaD probe. Confocal microscopy using (*c*) Nomarski optics or (*d*) 700 nm fluorescence emission of CaD+ cell culture 1 h after incubation with the reporter probe ($\times$200 magnification). Note that the NIRF signal in *d* clearly originates from vesicular structures within the cells, presumably the lysosomal compartment. No signal was observed when control probes containing nonsense peptide spacers were used (data not shown).

appropriate excitation and emission filters (650/700 nm; Omega Optical). Sections were viewed in phase-contrast or NIRF mode using an inverted epifluorescence microscope (Zeiss Axiovert, Thornwood, NY), and images were obtained with a cooled CCD camera (Sensys; Photometrics, Tuscon, AZ) interfaced to a Macintosh computer.

RESULTS

***In Vitro* Characterization.** RT-PCR analysis of the rodent tumor model showed that CaD+ cells grown in culture or *in vivo* contained hCaD mRNA message (Fig. 2*a*). The mock-transfected control cell line (CaD−) and whole CaD− tumors were negative for mRNA expression. Western blotting of the CaD+ cells showed a faint band at M_r 52,000 (proCaD) and a pronounced band at M_r 34,000 (activated CaD; Fig. 2*b*).

In vitro, the synthesized CaD probe was essentially optically "silent," generating <1 AU at 675 nm excitation and 694 nm emission, whereas the CaD activated probe generated over 60-fold higher fluorescence. To test for the specificity of activation, we also compared the probe with a scrambled peptide containing the same amino acids but in a different sequence. As shown in Fig. 3*a*, there was essentially no NIRF activation with the control probe when incubated with purified hCaD. To test for the linearity of NIRF signal generation, the probe was also incubated with different amounts of CaD+ cells (Fig. 3*b*). The measured NIRF signal was linear over a range of at least 4 orders of magnitude ($r^2 = 0.99$; Fig. 3*b*). When CaD+ cells incubated with the probe for 1 h were observed by confocal fluorescence microscopy, a NIRF signal could be seen originating from vesicular structures within cells, presumably representing the lysosomal compartment (Fig. 3, *c* and *d*). No detectable signal was observed when control probes containing nonsense peptide spacers were used. Likewise, no signal was observed when CaD− cells were used.

***In Vivo* Imaging.** When the probe was administered i.v. to tumor-bearing mice, no apparent signs of toxicity were seen, similar to that observed for other PGC-based compounds (11). A clearly detectable NIRF signal was observed from all CaD+ tumors in live animals, and a representative image sequence is shown in Fig. 4. The CaD+ tumors always emitted much higher fluorescence than the matched CaD− tumors. Mean signal intensities and CNRs are summarized in Table 1. The mean CNR for tumor periphery CaD+ tumors compared with CaD− tumors was 8.6, whereas the center of CaD+ tumors compared with CaD− tumors resulted in a CNR of 6.0. The CNR of CaD+ periphery and center compared to nontarget tissue was 22.8 and 16.2, respectively. The differences between mean SI for tumor periphery of CaD+ compared with entire CaD− tumors and for tumor center of CaD+ compared with entire CaD− tumors were highly significant ($P < 0.001$ and $P < 0.005$, respectively), as was the comparison of CaD+ tumor periphery and center with background tissue ($P < 0.001$ for both).

Ex vivo NIRF images of the paired tumors obtained from the same animal (Fig. 5) confirmed the marked differences in probe activation between CaD+ and CaD− tumors. Heterogeneity of tumoral NIRF signal was observed *in vivo*, in excised tumor specimen (Fig. 5), and also in histological sections (Fig. 6). CaD expression was commonly highest in the periphery of tumors, in intratumoral septae, and in focal nodular areas with high growth rates. A similar finding has also been observed previously for other proteases when studied in tumor chamber models by intravital microscopy (data not shown). The morphological appearance of the tumors and their vascular density were similar by histology.

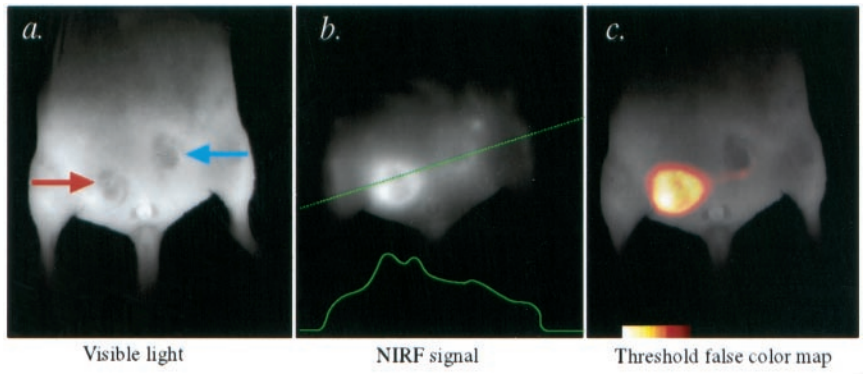

Fig. 4. Representative optical images of the lower abdomen of a nude mouse implanted with a CaD+ (*red arrow*) and CaD− (*blue arrow*) tumor. *a*, white light image 24 h after i.v. injection of the reporter probe. *b*, identical imaging set-up as in *a*, except that NIRF fluorescence is shown at 700 nm. Note that the CaD+ tumor emits fluorescence, whereas the CaD− tumor has a significantly lower signal. The *dotted green line* represents the line for the density slice profile shown at the bottom. *c*, superimposed images from *a* and *b*, with CaD information shown as a thresholded false color map.

Table 1 *SI and CNRs for tumor regions*

Region of interest	SI mean ± SD (AU)	CNR	*P*
CaD+, periphery	59,100 ± 1,500	NA	
CaD+, center	52,600 ± 1,500	NA	
CaD−, tumor	35,300 ± 5,200	NA	
Nontarget tissue[a]	23,000 ± 1,700	NA	
CaD+ periphery to CaD−	NA[b]	8.6	<0.001
CaD+ center to CaD−	NA	6.0	<0.005
CaD+ periphery to background	NA	22.8	<0.001
CaD+ center to background	NA	16.2	<0.001

[a] Observed NIRF signal originates from endogenous fluorochromes (autofluorescence) and exogenous (*i.e.*, diet) fluorochromes. CNR = $(SI_1 - SI_2)/\sqrt{(SD_1^2 + SD_2^2)}$.
[b] NA, not applicable.

DISCUSSION

Proteases are essential for the normal functioning of mammalian cells (15), bacteria (16), and viruses (17). Analysis of several genomes has shown that about 2% of all gene products are proteases (15). Proteases also play key roles in many diseases including neoplastic (18–20), vascular (21), infectious (22), degenerative (23), and autoimmune disorders (24). Given their central role, proteases have received considerable attention as therapeutic drug targets (22, 25, 26). The ability to evaluate specific enzyme activity *in vivo* would thus have considerable clinical and basic science applications. For example, protease imaging could be used to improve the early detection of diseases (4), to image the efficacy of protease inhibitors, to serve as an *in vivo* screening tool for drug development, to image transgene expression, or to understand how protease activities are regulated in intact micro- and macroenvironments. Thus far, detection of enzyme activity has been limited to *ex vivo* assays on excised tissues or fluid samples using fluorescence detection kits, immunohistology, ELISA, or Western blotting or to radiolabeled enzyme substrates.

The primary goal of the current study was to investigate whether a given single protease could be detected noninvasively by *in vivo* imaging. Although the model system used in this study may be somewhat artificial (overexpression of a transgene), our results clearly confirm the feasibility of the approach. CaD, an aspartic lysosomal protease, was chosen as a target protease because of the availability of CaD+ and CaD− tumor models (8, 9), the fact that the enzyme is primarily localized in the lysosomal compartment of cells (8) into which the graft copolymer is internalized (7, 11), and because of the potential role of the enzyme in metastasis formation (8) and local invasiveness (27). Early detectable NIRF signals emanated from the CaD+ tumors both *in vivo* and *ex vivo* and by microscopy. Interestingly, *in vivo* CaD expression in experimental tumors was somewhat heterogeneous and preferentially occurred in the tumor periphery, well-vascularized septae traversing the tumor, and/or focal areas with high cell turnover. Although it is conceivable that the CaD+ and CaD− tumors may have slightly different vascular permeabilities, prior research has shown that the developed graft copolymers distribute evenly in the steady state, unless VEGF is markedly up-regulated, for example, such as in transfected tumor models (28). Even if local accumulation of the nonactivated probe in the interstitium was heterogeneous, this would be undetectable by NIRF imaging because the probe has not yet been activated (note also the absence of NIRF signal in the blood, where probe concentration is relatively high; Fig. 6).

The developed protease reporter probe was based on a synthetic graft copolymer (partially methoxy-polyethylene glycol-modified poly-L-lysine) originally developed as a long-circulating drug carrier with circulation times in excess of 36 h in rodents and 20 h in humans (6, 11, 29). The graft copolymer is slowly internalized into proliferating tumor cells (7, 11) and has thus been used for chemotherapeutic drug delivery (30). The CaD-specific peptide (5) used in this study consisted of the Gly-Pro-Ile-Cys(Et)-Phe-Phe-Arg-Leu-Gly-Lys(FITC)-Cys-NH_2 sequence. Given the modular design of the reporter probe, the peptide sequence could easily be replaced with sequences specific for other proteases. For example, fairly specific peptide substrates have been described for caspases (31), MMPs (32), viral proteases (33), or prostate specific antigen, an intracellular serine protease (34). Future developments of imaging probes against these and other targets would be of considerable clinical value.

The NIRF fluorochrome chosen for this study was an indocyanine compound (Cy5.5) with an emission maximum at 694 nm. The NIR wavelength of excitation and emission was chosen to improve tissue penetration compared with fluorochromes active in the visible light range (35). The use a number of other fluorochromes with excitations/emissions at even longer wavelengths (700–1000 nm) to further decrease attenuation by tissues and potentially enable multichannel imaging in the NIR spectrum is conceivable. The second reason for using indocyanine fluorochromes was their generic ability to efficiently quench when in close spatial proximity to each other, thus avoiding the need for dedicated quenchers such as 4-(4′-dimethylaminophenylazo)benzoic acid used in other molecular beacon approaches (1). In prior research, we had optimized the number of fluorochromes per PGC for maximum quenching to occur and shown that at least 10 molecules are required (4). In the current study, 22 fluorochromes were positioned on peptide stalks on each PGC, which is the reason for the extremely low signal of the reporter in its native state and the intense fluorescence in the activated state (12).

NIRF signal generation in this study was detected by using CCD technology, either in the form of microscopy or whole animal imaging (14). The latter was done with a planar imaging system, using a continuous excitation source and a long pass filter to record emission at >700 nm. Because we used a long pass rather than a bandpass filter to record generated fluorescence, the native background signal was high from both reflected excitation photons not filtered due to the slight overlap of filter frequency cutoff tails and other native fluorochromes with emission >700 nm. The more recent use of narrow bandpass filters (705–715 nm) and the simultaneous use of polarization filters have further decreased nonspecific background. Although

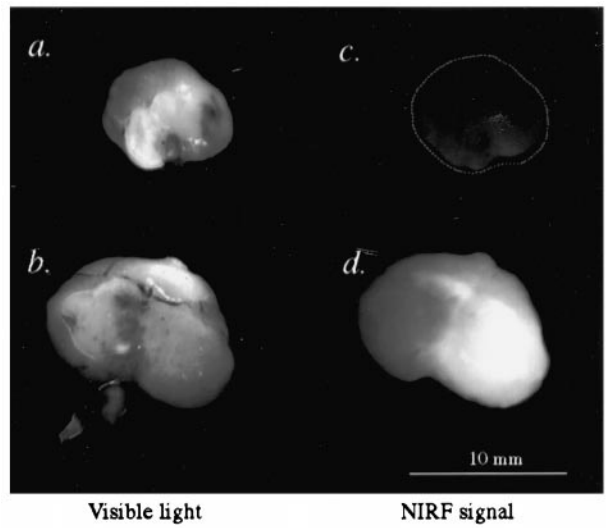

Fig. 5. Excised CaD− (*a*) and CaD+ (*b*) tumors from an animal 24 h after i.v. injection of the reporter probe. Note the significant NIRF signal generation in the CaD+ tumor (*d*) and the near absence of signal in the CaD− tumor (*c*; identical imaging settings). The NIRF signal in the CaD+ tumor is heterogeneous.

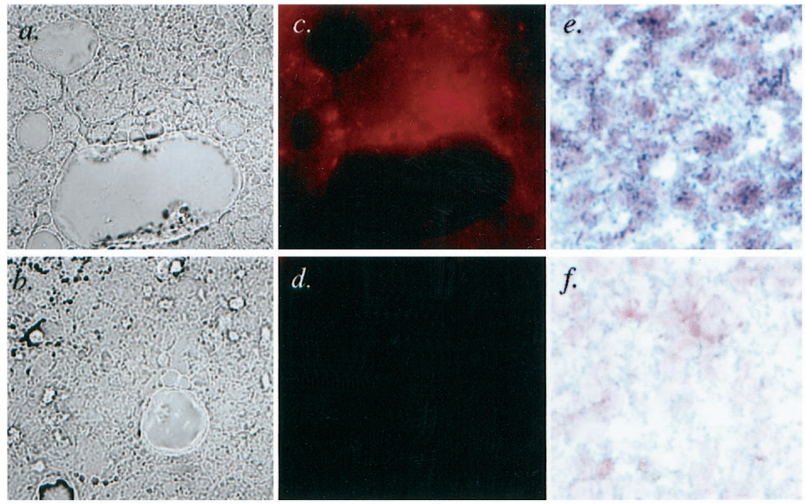

Fig. 6. Composite histological sections from excised tumors of animals injected i.v. with the reporter probe. The first column of images represents phase-contrast images of unstained sections of CaD+ (*a*) and CaD− (*b*) tumors. The middle column represents the same sections at 700 nm fluorescence (×200). Note the NIRF signal generation from within cells in the CaD+ tumor (*c*). The larger featureless areas represent vessels. CaD+ (*e*) and CaD− (*f*) tumor stained with anticathepsin and revealed with alkaline phosphatase reaction (*blue* pigment; Kernecht counterstain; ×600).

this prototype imaging system is useful for fast, high-resolution screening of superficial events, it generally does not allow adequate detection of photons from deep tissues (*i.e.*, >10 mm deep). If the latter is required (as in the clinical scenario, unless endoscopic imaging is performed), different NIR optical detection systems have to be used. Such systems can be based on phase modulation signal (36, 37), diffuse optical tomography (38), or ultrafast imaging of ballistic and/or early arriving photons (39). As these innovative imaging approaches enter the realm of clinical testing, it will become apparent that there will be sufficient SI from deep tissues when used with the developed probes (40).

The current study indicates that the autoquenched probe is specific *in vivo*. Although the detection threshold of the probe was not directly determined in this study, Cy5.5 concentrations in the nanomolar range have been previously detectable (4). With a more sensitive detection system such as phase array technology (36), the detection threshold is expected to be in the picomolar range in deep tissue. Recalculating these detection thresholds, it is entirely feasible to reach locally high enough substrate concentrations at physiologically acceptable doses of fluorochromes. Although the dose used in this rodent study would scale up to 175 mg of drug substance in a human, it is at least 2–3 orders of magnitude above the theoretical detection threshold. Fluorochromes such as indocyanine green are used routinely in cardiology, hepatology, ophthalmology, and, most recently, clinical diffuse optical tomography imaging (40) at i.v. doses of 25–50 mg.

Although the current study used CaD as a model protease, a variety of other proteases are highly relevant in oncological and cardiovascular imaging (18, 19). The next logical step will be to identify a clinically relevant protease and design a similar probe for clinical testing. Ideally, the probe would be tested in a protease inhibitor trial to monitor real-time drug efficacy at the molecular level. To this extent, we have synthesized a MMP-2-sensitive probe and shown that MMP-2 inhibitor treatment can indeed be monitored by this approach.

In summary, the use of reporter probes to noninvasively image enzyme activity has been demonstrated *in vivo*. One of the main utilities of the technique is expected to lie in the evaluation of the large number of metalloprotease and HIV protease inhibitors currently under development and/or in clinical use. As we move forward to design and build imaging probes with molecular specificity, new applications are likely to occur such as *in vivo* imaging of transgenes or screening of potential drug candidates.

ACKNOWLEDGMENTS

We thank Dr. A. Bogdanov for helpful discussions and for providing the protected graft copolymer, Drs. H. Rochefort and M. Garcia for providing the 3Y1 cell lines, Drs. N. Michaud and C. Lin for help with confocal microscopy experiments, and Dr. M. Lewin for Western blotting. We also thank Drs. J. Basilion and L. Josephson for many helpful discussions and review of the manuscript.

REFERENCES

1. Tyagi, S., and Kramer, F. R. Molecular beacons: probes that fluoresce upon hybridization. Nat. Biotechnol., *14:* 303–308, 1998.
2. Zlokarnik, G., Negulescu, P. A., Knapp, T. E., Mere, L., Burres, N., Feng, L., Whitney, M., Roemer, K., and Tsien, R. Y. Quantitation of transcription and clonal selection of single living cells with β-lactamase as reporter. Science (Washington DC), *279:* 84–88, 1998.
3. Packard, B. Z., Toptygin, D. D., Komoriya, A., and Brand, L. Profluorescent protease substrates: intramolecular dimers described by the exciton model. Proc. Natl. Acad. Sci. USA, *93:* 11640–11645, 1996.
4. Weissleder, R., Tung, C. H., Mahmood, U., and Bogdanov, A. *In vivo* imaging of tumors with protease-activated near-infrared fluorescent probes. Nat. Biotechnol., *17:* 375–378, 1999.
5. Gulnik, S. V., Suvorov, L. I., Majer, P., Collins, J., Kane, B. P., Johnson, D. G., and Erickson, J. W. Design of sensitive fluorogenic substrates for human cathepsin D. FEBS Lett., *413:* 379–384, 1997.
6. Callahan, R., Bogdanov, A., Fischman, A., Brady, T., and Weissleder, R. Preclinical evaluation and Phase I clinical trial of a 99mTc labeled synthetic polymer used in blood pool imaging. Am. J. Roentgenol., *171:* 137–143, 1998.
7. Marecos, E., Weissleder, R., and Bogdanov, A., Jr. Antibody-mediated *versus* non-targeted delivery in a human small cell lung carcinoma model. Bioconjug. Chem., *9:* 184–191, 1998.
8. Garcia, M., Derocq, D., Pujol, P., and Rochefort, H. Overexpression of transfected cathepsin D in transformed cells increases their malignant phenotype and metastatic potency. Oncogene, *5:* 1809–1814, 1990.
9. Garcia, M., Platet, N., Liaudet, E., Laurent, V., Derocq, D., Brouillet, J., and Rochefort, H. Biological and clinical significance of cathepsin D in breast cancer metastasis. Stem Cells, *14:* 642–650, 1995.
10. Rochefort, H., and Liaudet-Coopman, E. Cathepsin D in cancer metastasis: a protease and a ligand. APMIS, *107:* 86–95, 1999.
11. Bogdanov, A., Jr., Wright, S. C., Marecos, E. M., Bogdanova, A., Martin, C., Petherick, P., and Weissleder, R. A long-circulating co-polymer in "passive targeting" to solid tumors. J. Drug Target., *4:* 321–330, 1997.
12. Tung, C. H., Bredow, S., Mahmood, U., and Weissleder, R. Preparation of a cathepsin D sensitive near infrared fluorescence probe for imaging. Bioconjug. Chem., *10:* 892–896, 1999.
13. Liu, Z., Brattain, M. G., and Appert, H. Differential display of reticulocalbin in the highly invasive cell line, MDA-MB-435, *versus* the poorly invasive cell line, MCF-7. Biochem. Biophys. Res. Commun., *231:* 283–289, 1997.
14. Mahmood, U., Tung, C., Bogdanov, A., and Weissleder, R. Near infrared optical imaging system to detect tumor protease activity. Radiology, *213:* 866–870, 1999.
15. Barrett, A. J., Rawlings, N. D., and Woessner, J. F. (eds.). Handbook of Proteolytic Enzymes. New York: Academic Press, 1998.
16. Gottesman, S. Regulation by proteolysis: developmental switches. Curr. Opin. Microbiol., *2:* 142–147, 1999.
17. Greber, U. F. Virus assembly and disassembly: the adenovirus cysteine protease as a trigger factor. Rev. Med. Virol., *8:* 213–222, 1998.

18. Sloane, B. F. Suicidal tumor proteases. Nat. Biotechnol., *14:* 826–827, 1996.
19. Koblinski, J. E., Ahram, M., and Sloane, B. F. Unraveling the role of proteases in cancer. Clin. Chim. Acta, *291:* 113–135, 2000.
20. Kugler, A. Matrix metalloproteinases and their inhibitors. Anticancer Res., *19:* 1589–1592, 1999.
21. Sun, A., and Cheng, J. Novel targets for therapeutic intervention against ischemic brain injury. Clin. Neuropharmacol., *22:* 164–171, 1999.
22. Kaul, D. R., Cinti, S. K., Carver, P. L., and Kazanjian, P. H. HIV protease inhibitors: advances in therapy and adverse reactions, including metabolic complications. Pharmacotherapy, *19:* 281–298, 1999.
23. Ona, V. O., Li, M., Vonsattel, J. P., Andrews, L. J., Khan, S. Q., Chung, W. M., Frey, A. S., Menon, A. S., Li, X. J., Stieg, P. E., Yuan, J., Penney, J. B., Young, A. B., Cha, J. H., and Friedlander, R. M. Inhibition of caspase-1 slows disease progression in a mouse model of Huntington's disease. Nature (Lond.), *399:* 263–267, 1999.
24. Benveniste, E. N. Role of macrophages/microglia in multiple sclerosis and experimental allergic encephalomyelitis. J. Mol. Med., *75:* 165–173, 1997.
25. Kahari, V. M., and Saarialho-Kere, U. Matrix metalloproteinases and their inhibitors in tumour growth and invasion. Ann. Med., *31:* 34–45, 1999.
26. Sanderson, P. E. Small, noncovalent serine protease inhibitors. Med. Res. Rev., *19:* 179–197, 1999.
27. Liaudet, E., Derocq, D., Rochefort, H., and Garcia, M. Transfected cathepsin D stimulates high density cancer cell growth by inactivating secreted growth inhibitors. Cell Growth Differ., *6:* 1045–1052, 1995.
28. Lewin, M., Bredow, S., Sergeyev, N., Marecos, E., Bogdanov, A., Jr., and Weissleder, R. *In vivo* assessment of vascular endothelial growth factor-induced angiogenesis. Int. J. Cancer, *83:* 798–802, 1999.
29. Bogdanov, A., Weissleder, R., and Brady, T. Long-circulating blood pool imaging agents. Adv. Drug Delivery Rev., *16:* 335–348, 1995.
30. Bogdanov, A., Martin, C., Bogdanova, A. V., Brady, T. J., and Weissleder, R. An adduct of *cis*-diamminedichloroplatinum(II) and poly(ethylene glycol)poly(L-lysine)-succinate: synthesis and cytotoxic properties. Bioconjug. Chem., *7:* 144–149, 1996.
31. Cohen, G. M. Caspases: the executioners of apoptosis. Biochem. J., *326:* 1–16, 1997.
32. Netzel-Arnett, S., Mallya, S. K., Nagase, H., Birkedal-Hansen, H., and Van Wart, H. E. Continuously recording fluorescent assays optimized for five human matrix metalloproteinases. Anal. Biochem., *195:* 86–92, 1991.
33. Sardana, V. V., Wolfgang, J. A., Veloski, C. A., Long, W. J., LeGrow, K., Wolanski, B., Emini, E. A., and La Femina, R. L. Peptide substrate cleavage specificity of the human cytomegalovirus protease. J. Biol. Chem., *269:* 14337–14340, 1994.
34. Denmeade, S., Lou, W., Lovgren, J., Malm, J., Lilja, H., and Isaacs, J. Specific and efficient peptide substrates for assaying the proteolytic activity of prostate-specific antigen. Cancer Res., *57:* 4924–4930, 1997.
35. Hoshi, Y., Hazeki, O., Kakihana, Y., and Tamura, M. Redox behavior of cytochrome oxidase in the rat brain measured by near-infrared spectroscopy. J. Appl. Physiol., *83:* 1842–1848, 1997.
36. Chance, B. Near-infrared images using continuous, phase-modulated, and pulsed light with quantitation of blood and blood oxygenation. Ann. N. Y. Acad. Sci., *838:* 29–45, 1998.
37. Kang, K. A., Bruley, D. F., Londono, J. M., and Chance, B. Localization of a fluorescent object in highly scattering media via frequency response analysis of near infrared-time resolved spectroscopy spectra. Ann. Biomed. Eng., *26:* 138–145, 1998.
38. Boas, D. A., O'Leary, M. A., Chance, B., and Yodh, A. G. Scattering of diffuse photon density waves by spherical inhomogeneities within turbid media: analytic solution and applications. Proc. Natl. Acad. Sci. USA, *91:* 4887–4891, 1994.
39. Wu, J., Perelman, L., Dasari, R., and Feld, M. Fluorescence tomographic imaging in turbid media using early-arriving photons and Laplace transforms. Proc. Natl. Acad. Sci. USA, *94:* 8783–8788, 1997.
40. Ntziachristos, V., Yodh, A. G., Schnall, M., and Chance, B. Concurrent MRI and diffuse optical tomography of breast after indocyanine green enhancement. Proc. Natl. Acad. Sci. USA, *97:* 2767–2772, 2000.